HINS R&D Collaboration on Electron Cloud Effects: Build-Up Simulations at the Electron Detector Location in the MI*

M. A. Furman†
Center for Beam Physics
Lawrence Berkeley National Laboratory, Bldg. 71R0259
1 Cyclotron Rd.
Berkeley, CA 94720
(Dated: Dec. 5, 2006)

We present a report on ongoing simulations in the context of the HINS [1] activities on electron-cloud effects for the MI upgrade [2–5]. The present report pertains only to electron-cloud build-up simulations at the location of the electron detector. Our results seem to show a significantly stronger electron-cloud effect than observed. However, the sensitivity of our results to several important variables remains to be explored in order to reach any firm conclusions from the comparison against measurements.

I. ASSUMPTIONS.

For the MI conditions relevant to the electron detector measurements, we make the following assumptions [6]:

A. Fill pattern.

We assume a MI bunch fill pattern as follows:

(82*H)(4*0)(82*L)(4*0)(82*L)(4*0)(82*L)(4*0)(82*L)(4*0)(82*L)(76*0)

where each component of the form (n^*N_b) represents a sequence of n buckets of intensity N_b, where H means $N_b = 10.3 \times 10^{10}$, L means $N_b = 5.7 \times 10^{10}$, and 0 means $N_b = 0$.

B. Beam energies and bunch sizes.

We have carried out simulations for six cases, namely beam kinetic energy $K = 8$, 20 and 30 GeV, and 2 values for the RMS bunch length σ_z for each value of K, as listed in Tab. I below. The chosen values for σ_z are meant to approximately represent the RMS bunch length at the corresponding energy during the ramp.

We assume a normalized 95% transverse emittance $\epsilon_{n,95\%} = 15\pi$ mm-mrad for all bunches for all 6 cases. Assuming that the beta functions at the electron detector location are $(\beta_x, \beta_y) = (20, 30)$ m, and assuming negligible dispersive beam width, we obtain the values listed in Tab. I for the RMS transverse beam sizes.

C. Beam pipe.

We assume that, at the electron detector location, the pipe is round with radius 73 mm and there is no magnetic field. We assume, for the purposes of parameter exploration, that the peak SEY $\delta_{\max}$ is in the range 1.3–1.7. We further assume the stainless steel SEY model described in [7, 8], with the additional practical assumption that the SEY at 0 energy, $\delta(0)$, is proportional to $\delta_{\max}$, as discussed in more detail below.

---

*Work supported by the FNAL HINS R&D Effort and by the US DOE under contract DE-AC02-05CH11231.
†Electronic address: mafurman@lbl.gov; URL: http://mafurman.lbl.gov

TABLE I: Assumed beam parameters.

Beam kinetic energy	K [GeV]	8	20	30
Beam relativistic factor	γ_b	9.486	22.32	32.97
95% bunch duration	T_b [ns]	8 or 6	1 or 0.75	1.8 or 1.5
RMS bunch length	σ_z [m]	0.596 or 0.447	0.0749 or 0.0562	0.135 or 0.112
Hor. RMS bunch size	σ_x [mm]	2.29	1.50	1.23
Vert. RMS bunch size	σ_y [mm]	2.81	1.83	1.51

II. RESULTS.

The simulations with the code POSINST [7–10] for a full machine revolution for $\delta_{\max} \geq 1.5$ have proven to be challenging, particularly for the cases when $K = 20$ or 30 GeV for which the relatively small σ_z lead to a strong electron-cloud effect. Initial simulations with relatively few macroelectrons and/or coarse time steps proved to be too noisy. The results presented here were achieved with an integration time step Δt in the range $(1.4 - 15) \times 10^{-11}$ s, a maximum number $M_e = 20,000$ of macroelectrons allowed at any given time, and a 64×64 space-charge grid. CPU running times on a Macintosh G5 (1.8 GHz) range from 1 to 7 hrs for one full MI revolution. Ideally, we would simulate the electron-cloud build-up and decay during the full MI ramp, lasting ~ 0.5 s. Given that the revolution period is ~ 11 μs, this amounts to ∼45,000 turns, clearly beyond present-day computer capabilities.

Figs. 1-3 show the build-up of the electron-cloud line density λ_e for the three values of K but only for the first (larger) value of σ_z considered for each case. For $\delta_{\max} = 1.3$ a saturation is reached at a much lower level than the beam neutralization level, namely 1.62 nC/m, but for $\delta_{\max} \geq 1.5$, average neutralization is reached or exceeded. These figures also show the incident electron flux J_e at the walls of the chamber (we checked that J_e at the location of the detector is essentially identical to the average of J_e over the entire chamber, despite the fact that the transverse beam shape is upright with an aspect ratio $(3/2)^{1/2} \simeq 1.2$, which breaks the cylindrical symmetry of the problem).

An approximate and useful empirical rule, relating the electron flux at the wall J_e to λ_e can be extracted from Fig. 4, namely $J_e = \kappa\lambda_e$, where $\kappa \simeq 6 \times 10^7$ m^{-1} s^{-1}. This value of κ is approximately independent of K, σ_z and $\delta_{\max}$, and it also seems to be constant in time during the passage of the beam, as it can inferred from Fig. 1 (we have not tested the sensitivity of κ to N_b, however). A similar empirical rule has been found for LHC simulations [11].

Figs. 4-6 show the one-turn averages for various quantities plotted vs. $\delta_{\max}$, for all cases considered. Although the overall electron-cloud density is seen to exceed the beam neutralization level by up to a factor of ~ 2, the electron-cloud density within the 1-σ beam ellipse is only a few percent of the local beam neutralization level, $N_b/(\pi\sigma_x\sigma_y s_b)$, which is in the range $(0.5 - 1.7) \times 10^{15}$ m^{-3} for the cases considered (s_b is here the bunch spacing).

III. DISCUSSION.

The electron detector has a radius of 1.27 cm and an area duty factor of 30%, which yields an effective area $S = \pi \times 1.27^2 \times 0.30 = 1.5$ cm^2. The measured electron current [12, 13] is $I_e \simeq 0.1 - 0.3$ μA during acceleration, corresponding to a flux $J_e = I/S \sim (0.7 - 2) \times 10^{-3}$ A/m^2. Comparing this value with Figs. 1b and 4b, this would indicate $\delta_{\max} \gtrsim 1.4$ (in Fig. 4, J_e is in the range $1.8 \times 10^{-5} - 1.4 \times 10^{-3}$ for $\delta_{\max} = 1.4$).

Fig. 4b shows that J_e is much smaller for $K = 8$ GeV, especially for $T_b = 8$ ns, than for the other cases. This result is in qualitative agreement with observations. The result $\delta_{\max} \gtrsim 1.3$, however, appears to contradict the MI sample measurements carried out at SLAC [14], which show $\delta_{\max} \simeq 2$. However, our simulations may be sensitive to other model variables, which we have not yet explored, that may change our conclusions. For example, the value of the SEY at zero energy, $\delta(0)$, is likely to be significant. In all our simulations we have, for convenience, set $\delta(0)$ proportional to $\delta_{\max}$, namely $\delta(0) = 0.2438 \times \delta_{\max}$ [5]. A closely related issue is the relative composition of the secondary emission spectrum: different materials have different percentages of elastically backscattered, rediffused and true secondary electrons. The SEY model we have used is based on old measurements of the yield and spectrum for stainless steel samples, which show a relatively high contribution of rediffused electrons at all values of the incident energy E_0, not just for $E_0 \simeq 0$ [7, 8, 15]. These electrons are known to lead to a significant electron-cloud density [11] owing to somewhat indirect effects arising from their high emission energy relative to E_0. We do not know if our assumed emission spectrum composition actually corresponds to the recent MI sample measurements [14]. If our simulations were to be repeated under the assumption of an emission spectrum corresponding to copper, as opposed to stainless steel, the electron-cloud density would almost certainly be lower for a given value of $\delta_{\max}$ owing to the

lower fraction of rediffused electrons in copper. Since only rediffused and elastically backscattered electrons (but not true secondaries) contribute to $\delta(0)$, this quantity is a convenient measure of the effects from these electrons, and it seems important therefore to vary it independently of $\delta_{\max}$. In addition, the value of E_0 at which the SEY peaks, $E_{\max}$, can be important in some cases, but we have fixed it here at $E_{\max} = 293$ eV in all cases for convenience. This variable, therefore, also needs to be exercised.

In addition, it is possible that the 2D nature of our simulations may lead in some cases to stronger electron-cloud effects in field-free regions than what might be expected in reality. This is because in such regions electrons would be able to dissipate in the longitudinal direction provided the electron-cloud density is below space-charge saturation and there is enought time between successive bunch passages. This longitudinal dissipation is wholly absent in the 2D model embodied by POSINST, hence this mechanism needs to be assessed (this concern does not apply to dipole magnets or other magnetized regions because the magnetic field typically traps the electrons quite effectively in the transverse plane; it also does not apply to field-free regions when the electron cloud reaches a space-charge saturation).

The numerical instabilities seen at $\delta_{\max} = 1.5$ and 1.7 (Figs. 2-3) are not completely understood and deserve to be addressed. There are three ingredients in the simulation that contribute to such behavior, two of which are numerical issues and the third is a modeling issue. In the simulations presented here, we have limited the number of macroelectrons M_e at 20,000. This means that, whenever M_e exceeds 20,000 during the electron-cloud build-up, the simulation stops momentarily, half of the macroelectrons are randomly discarded, and the remaining half have their macro-charge (and -mass) renormalized in such a way that the total electron-cloud charge remains constant. Once this "culling" operation is completed, the simulation resumes. For higher values of $\delta_{\max}$, of course, culling happens more often than for low values. From simulations in other contexts, we have regularly observed that, if culling is suppressed so that the number of macroelectrons is allowed to grow unchecked, the numerical instabilities do not seem to arise. Unfortunately, such no-culling simulations are only possible for very short times or for low effective SEY, otherwise the number of macroelectrons grows to such an extent that computer memory is quickly exceeded.

A second, related, numerical issue that deserves clarification is the possible necessity of adjusting, perhaps locally, the space-charge grid size as the average macroelectron charge increases due to the culling process. We consistently observe that, when the electron cloud saturates due to the space-charge limit, macroelectrons tend to accumulate in thin layers very close to the chamber wall, leading to effects akin to virtual cathodes. While such space-charge saturation has a long research history, and is well understood in terms of analytic approaches for simplified geometries, we are not certain that the space-charge mesh we use, of fixed 64×64 size, is adequate to faithfully resolve the physics of such virtual cathodes, hence we do not know how much of this effect is physical or numerical. For example, the gradual increase of the charge of the macroelectrons near the wall due to culling, combined with a grid that does not adapt to the local charge density, might lead to an artificial enhancement of the image forces which, in turn, can exacerbate the virtual cathode effect.

The third ingredient that probably enters the observed instabilities is the possibly incomplete SEY model embodied in our code when space-charge forces are important. Our SEY model is implemented via a Monte Carlo process [7, 8] whose parameters are wholly insensitive to the space-charge forces that tend to push the just-born secondary electrons back to the wall. On the other hand, it seems to us reasonable to assume that the SEY might be suppressed, at least to some extent, when such forces are important. The non-suppression of the SEY in our model contributes, of course, to the accumulation of electrons near the walls. We are not aware of measurements of the SEY in the presence of an electric field pointing *away* from the surface, which must surely be exceedingly challenging. It is possible, however, that theoretical surface-physics arguments might be brought to bear in quantifying this suppression mechanism. An order-of-magnitude estimate of the space-charge field at the walls can be obtained under the assumption that the electron-cloud is uniformly distributed within the chamber, which leads to an electric field $E = \lambda_e/(2\pi\epsilon_0 R)$, where R is the chamber radius. In practical units, this yields E [V/m] $= (18\lambda_e$ [nC/m]$)/(R$ [m]). Assuming $\lambda_e = 4$ nC/m and $R = 0.07$ m, this yields $E = 1$ kV/m. However, local concentrations of electrons near the wall can lead to substantially different values for E.

IV. FUTURE GOALS.

In the near term we will carry out several tests that are straightforward extensions of the results presented here: we will explore the sensitivity of our results to the variables $E_{\max}$, $\delta(0)$, and the relative composition of the secondary emission spectrum. We will carry out 3D simulations with the code WARP/POSINST to quantify the importance of the longitudinal direction in the dissipation of the electron cloud. A longer-term R&D effort is the understanding of the numerical and physical ingredients that contribute to the appearance of the virtual cathodes, with the goal of an improved simulation model.

Acknowledgments

We are indebted to R. Zwaska for discussions and guidance on our work. We are grateful to NERSC for supercomputer support.

---

[1] Proton Driver Study. II. (Part 1, ch. 13), FERMILAB-TM-2169 (G. W. Foster, W. Chou and E. Malamud, eds.), May 2002.
[2] M. A. Furman, "A preliminary assessment of the electron cloud effect for the FNAL main injector upgrade," LBNL-57634/CBP-Note-712/FERMILAB-PUB-05-258-AD, 23 June 2006. A condensed version of this articled, of the same title, is published in New J. Phys. **8** (2006) 279. http://stacks.iop.org/1367-2630/8/279
[3] M. A. Furman, "Studies of e-cloud build up for the FNAL main injector and for the LHC," LBNL-60512/CBP Note-736, June 15, 2006; Proc. 39th ICFA Advanced Beam Dynamics Workshop on High Intensity High Brightness Hadron Beams "HB2006" (Tsukuba, Japan, May 29-June 2nd, 2006), paper TUAX05. http://hb2006.kek.jp/
[4] M. A. Furman, "HINS R&D Collaboration on Electron Cloud Effects: Midyear Progress Report," CBP-Technote-364/FERMILAB-TM-2369-AD, 22 Sept. 2006.
[5] M. A. Furman, K. Sonnad and J.-L. Vay, "HINS R&D Collaboration on Electron Cloud Effects: Midyear Report," LBNL-61921/CBP-761/FERMILAB-TM-2370-AD, Nov. 7, 2006.
[6] R. Zwaska, email dated 16 November 2006.
[7] M. A. Furman and M. T. F. Pivi, "Probabilistic model for the simulation of secondary electron emission," LBNL-49771/CBP Note-415 (Nov. 6, 2002). PRST-AB **5** 124404 (2003), http://prst-ab.aps.org/pdf/PRSTAB/v5/i12/e124404.
[8] M. A. Furman and M. T. F. Pivi, "Simulation of secondary electron emission based on a phenomenological probabilistic model," LBNL-52807/SLAC-PUB-9912 (June 2, 2003).
[9] M. A. Furman and G. R. Lambertson, "The electron-cloud instability in the arcs of the PEP-II positron ring," LBNL-41123/CBP Note-246, PEP-II AP Note AP 97.27 (Nov. 25, 1997). Proc. *Intl. Workshop on Multibunch Instabilities in Future Electron and Positron Accelerators "MBI-97"* (KEK, 15-18 July 1997; Y. H. Chin, ed.), KEK Proceedings **97-17**, Dec. 1997, p. 170.
[10] M. A. Furman, "The electron-cloud effect in the arcs of the LHC," LBNL-41482/CBP Note 247/LHC Project Report 180 (May 20, 1998).
[11] M. A. Furman and V. H. Chaplin, "Update on electron-cloud power deposition for the Large Hadron Collider arc dipoles," LBNL-59062/CBP Note 723 (January 30, 2006). PRST-AB **9** 034403 (2006), http://prst-ab.aps.org/pdf/PRSTAB/v9/i3/e034403
[12] R. Zwaska, "data," 21 June 2006.
[13] R. Zwaska, "Early slides," PPT file, 13 September 2006.
[14] R. Kirby, "SLAC SEY and Surface Analysis Measurements on FNAL Main Injector Ring S/S Beam Chamber Material," Sept. 5, 2006.
[15] R. E. Kirby and F. K. King, "Secondary Electron Emission Yields From PEP-II Accelerator Materials," SLAC-PUB-8212 (Oct. 2000). NIMPR A **469**, 1-12 (2001).

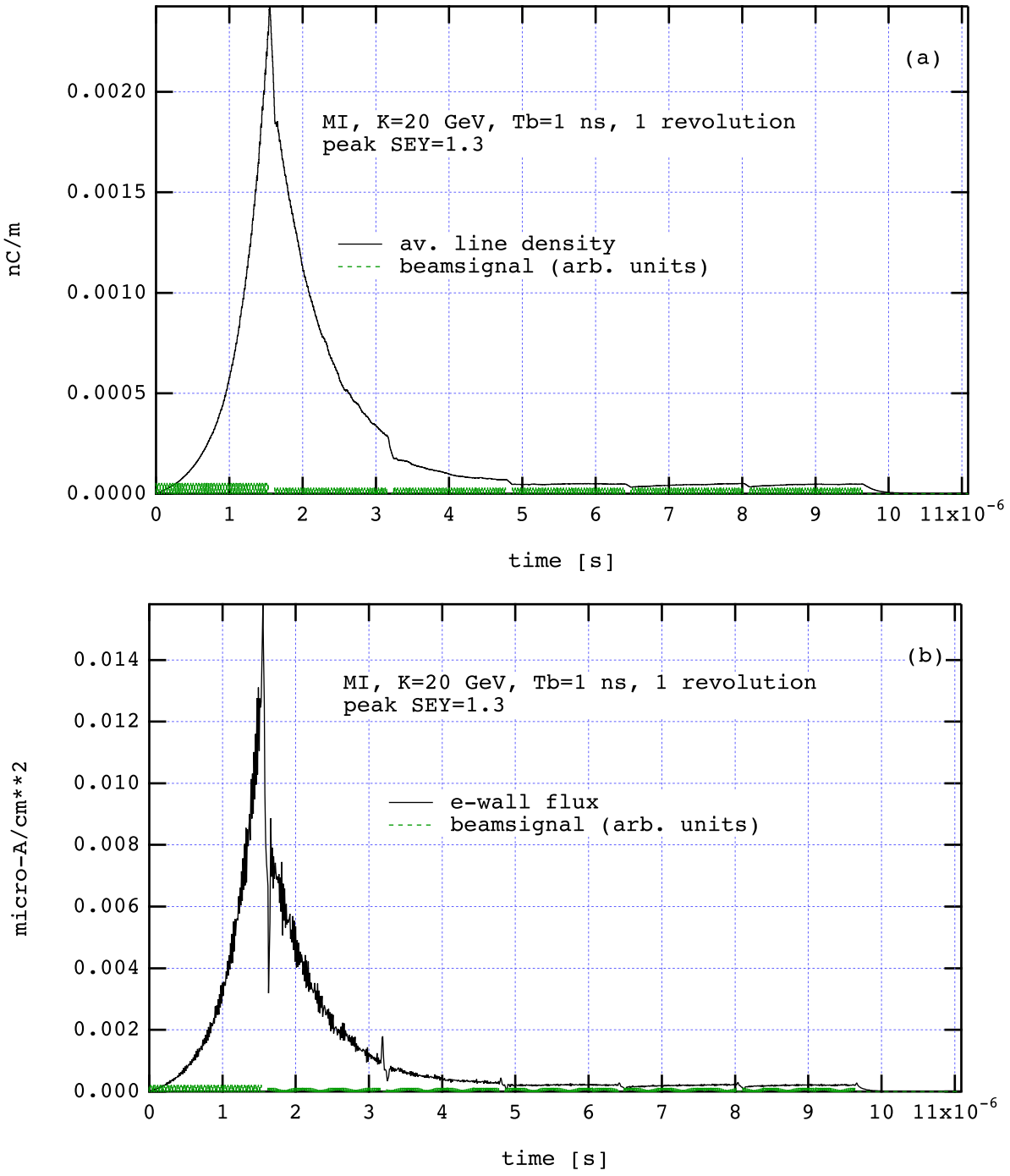

FIG. 1: electron cloud line density build-up and electron-wall flux for $K = 20$ GeV, $\delta_{\max} = 1.3$ and $T_b = 1$ ns.

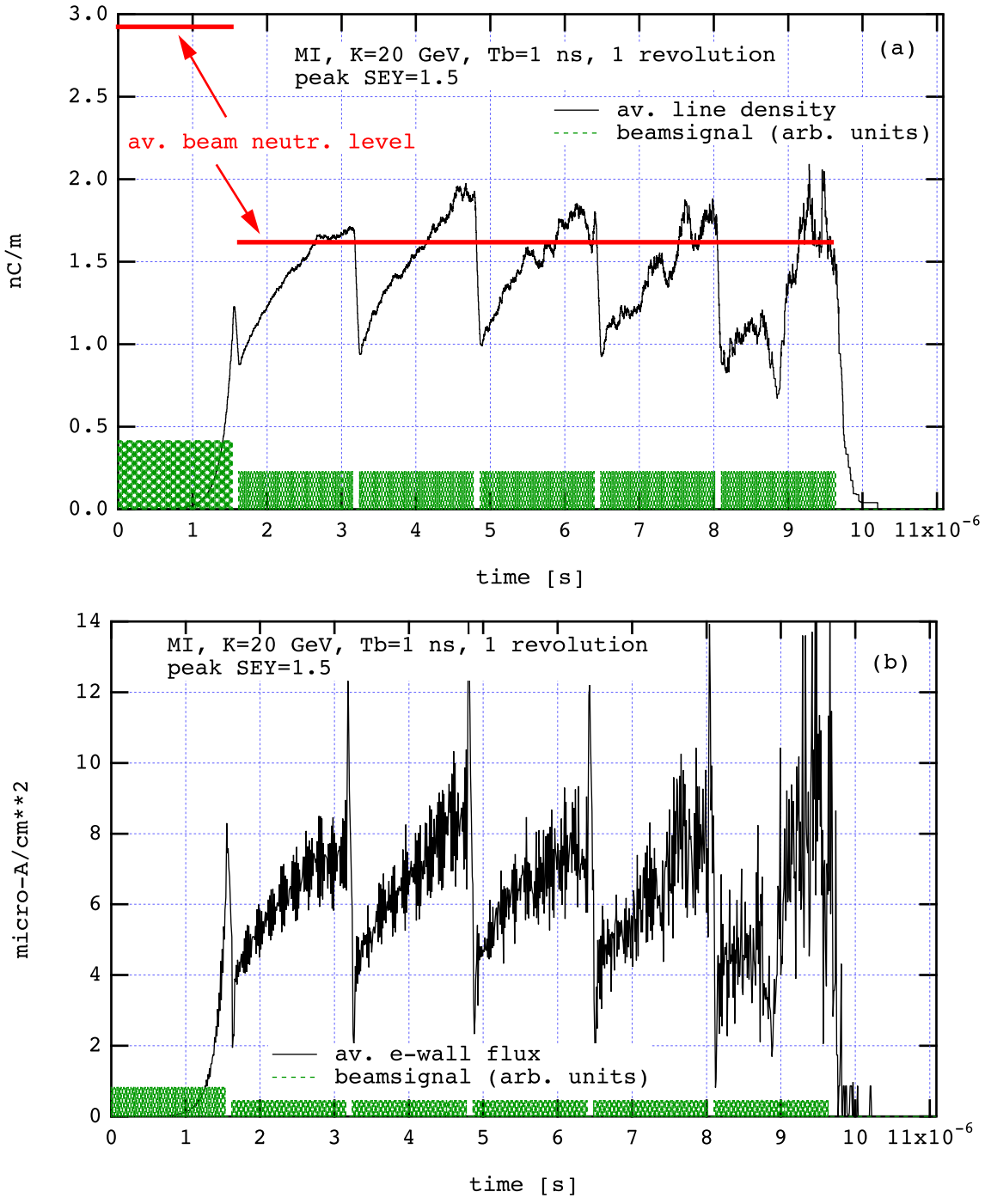

FIG. 2: electron cloud line density build-up and electron-wall flux for $K = 20$ GeV, $\delta_{\max} = 1.5$ and $T_b = 1$ ns.

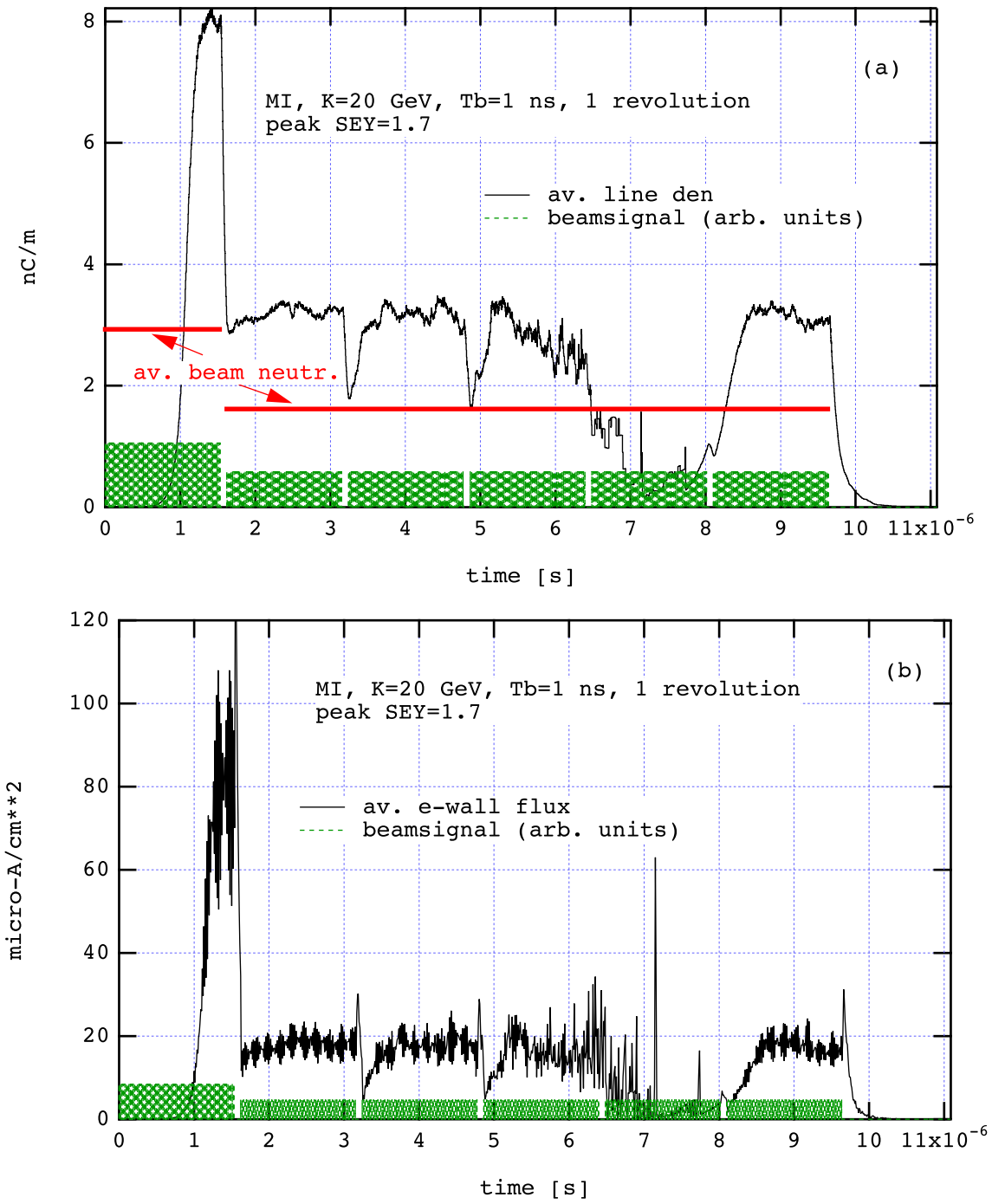

FIG. 3: electron cloud line density build-up and electron-wall flux for $K = 20$ GeV, $\delta_{\max} = 1.7$ and $T_b = 1$ ns. The large fluctuations seen at $t \sim 6 - 8$ μs are discussed in the text.

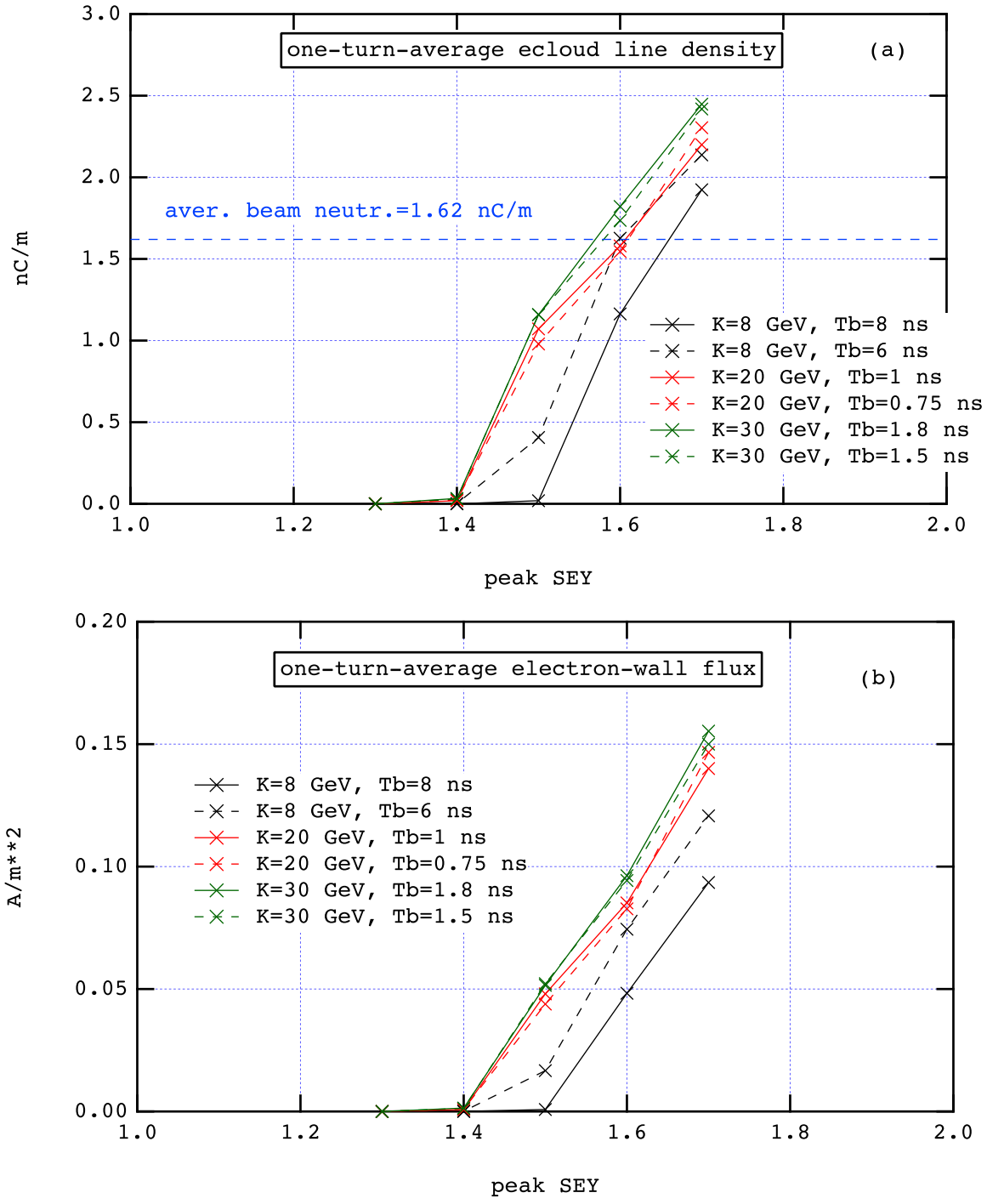

FIG. 4: One-turn-averaged electron cloud line density and electron flux at the wall. The beam neutralization level, $eN_b/s_b = 1.62$ nC/m, corresponds to the "L" batches ($1.6\ \mu s < t < 9.6\ \mu s$ in Figs. 1-3).

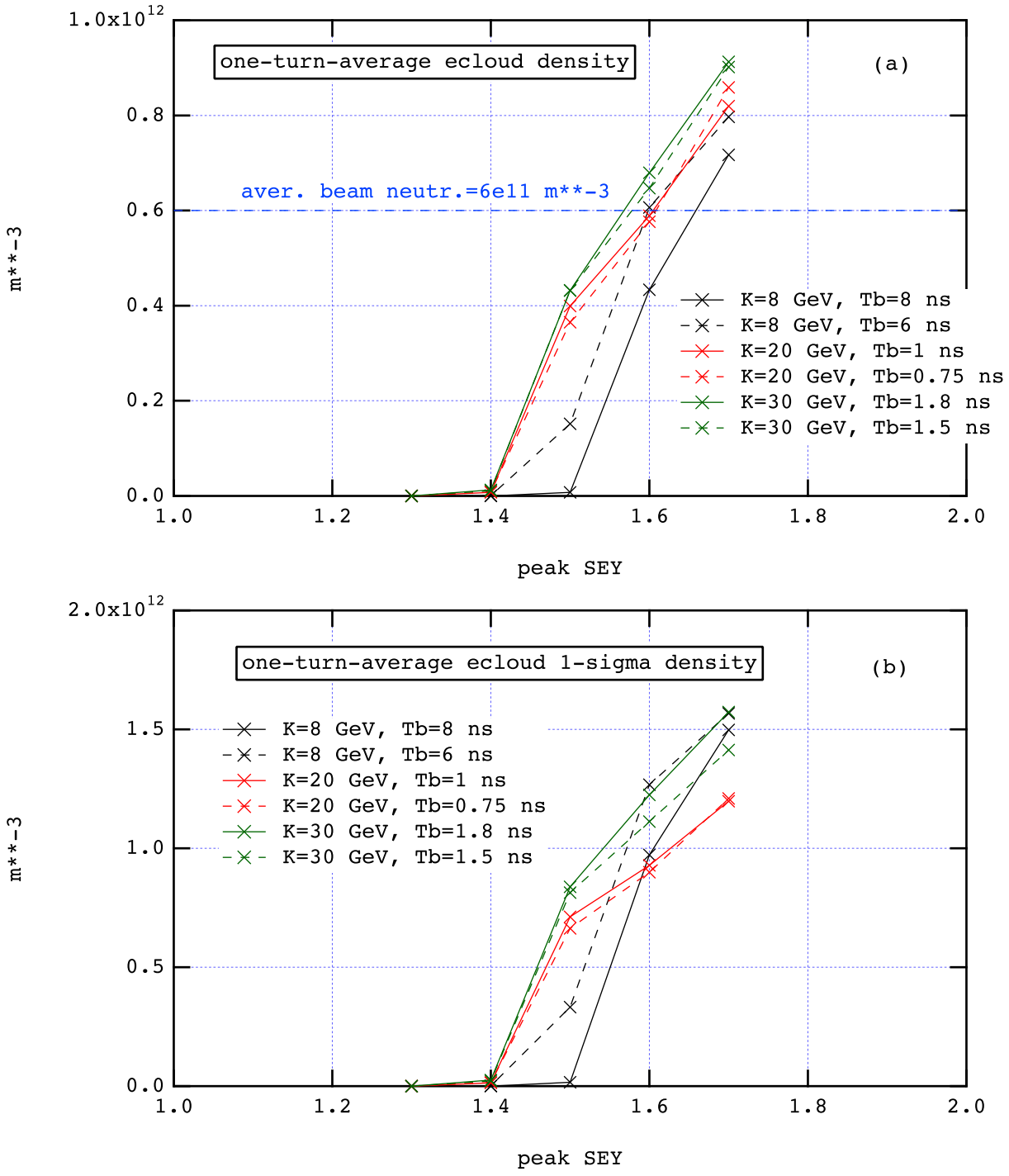

FIG. 5: One-turn-averaged electron cloud overall density and 1-σ density. The beam neutralization level, $N_b/(\pi abs_b) = 6\times10^{11}$ m^{-3}, corresponds to the "L" batches ($1.6\ \mu s < t < 9.6\ \mu$ s in Figs. 1-3). The 1-σ beam neutralization level is different for each case and ranges from 5×10^{14} m^{-3} for $K = 8$ GeV to 1.7×10^{15} m^{-3} for $K = 30$ GeV, i.e., it is much higher than the average electron cloud 1-σ density.

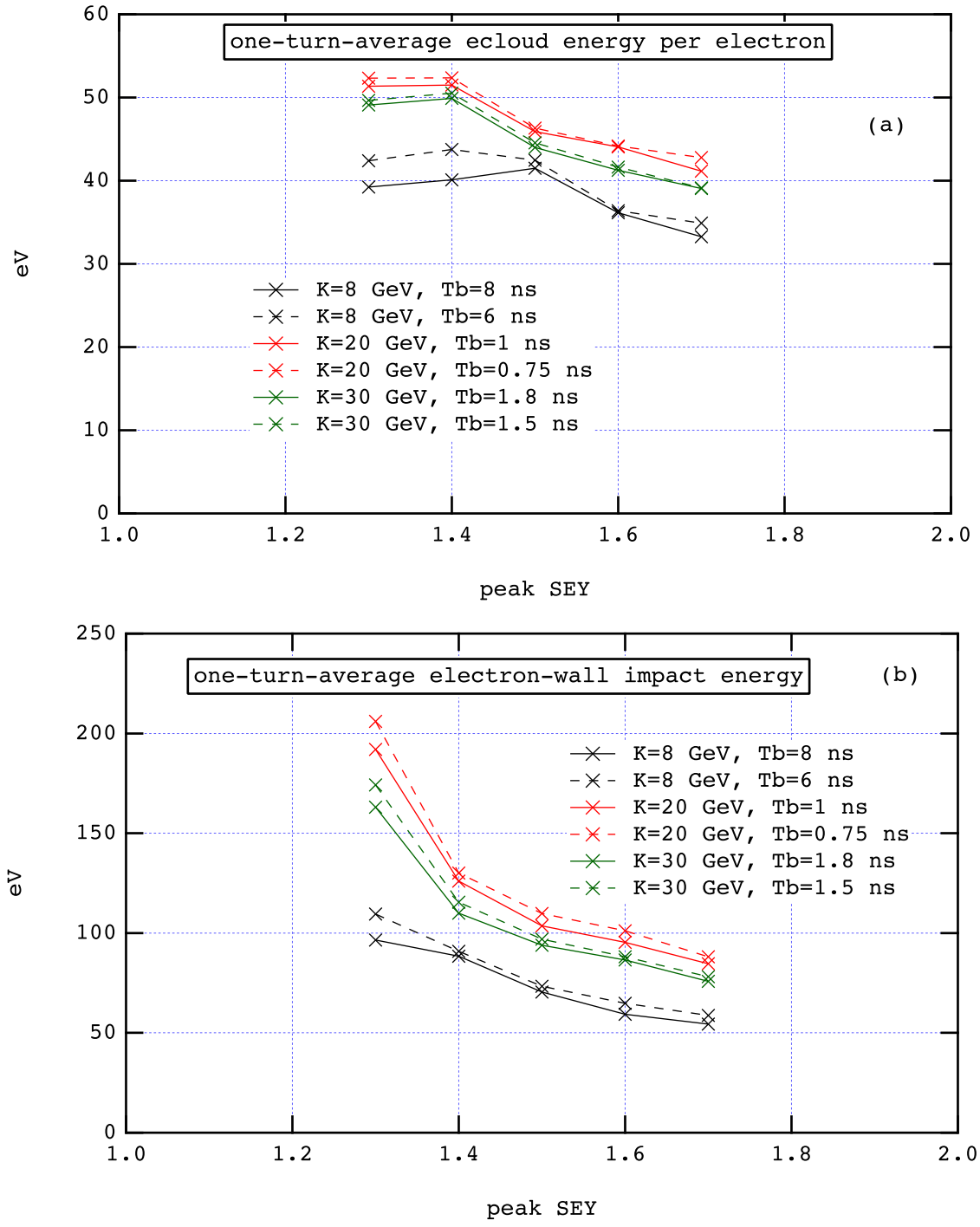

FIG. 6: One-turn-averaged electron energy and electron-wall impact energy.